Original Article

Deep-learning-based reconstruction of T2-weighted magnetic resonance imaging of the prostate accelerated by compressed sensing provides improved image quality at half the acquisition time

Martin Jurka[1], Iva Macova[1], Monika Wagnerova[1], Otakar Capoun[2], Roman Jakubicek[3], Petr Ourednicek[4], Lukas Lambert[1]^, Andrea Burgetova[1]^

[1]Department of Radiology, First Faculty of Medicine, Charles University and General University Hospital in Prague, Prague, Czech Republic; [2]Department of Urology, First Faculty of Medicine, Charles University and General University Hospital in Prague, Prague, Czech Republic; [3]Faculty of Electrical Engineering and Communication, Brno University of Technology, Brno, Czech Republic; [4]Department of Medical Imaging, St. Anna University Hospital Brno and Faculty of Medicine, Masaryk University, Brno, Czech Republic

Contributions: (I) Conception and design: I Macova, M Wagnerova, L Lambert, A Burgetova; (II) Administrative support: None; (III) Provision of study materials or patients: O Capoun, P Ourednicek, L Lambert; (IV) Collection and assembly of data: I Macova, M Wagnerova, O Capoun, L Lambert, A Burgetova; (V) Data analysis and interpretation: M Jurka, I Macova, M Wagnerova, R Jakubicek, L Lambert, A Burgetova; (VI) Manuscript writing: All authors; (VII) Final approval of manuscript: All authors.

Correspondence to: Prof. Lukas Lambert, MD, MSCS, PhD. Department of Radiology, First Faculty of Medicine, Charles University and General University Hospital in Prague, U Nemocnice 2, 128 08 Prague 2, Czech Republic. Email: lukas.lambert@vfn.cz.

Background: Deep-learning-based reconstruction (DLR) improves the quality of magnetic resonance (MR) images which allows faster acquisitions. The aim of this study was to compare the image quality of standard and accelerated T2 weighted turbo-spin-echo (TSE) images of the prostate reconstructed with and without DLR and to find associations between perceived image quality and calculated image characteristics.

Methods: In a cohort of 47 prospectively enrolled consecutive patients referred for bi-parametric prostate magnetic resonance imaging (MRI), two T2-TSE acquisitions in the transverse plane were acquired on a 3T scanner-a standard T2-TSE sequence and a short sequence accelerated by a factor of two using compressed sensing (CS). The images were reconstructed with and without DLR in super-resolution mode. The image quality was rated in six domains. Signal-to-noise ratio (SNR), and image sharpness were measured.

Results: The mean acquisition time was 281±23 s for the standard and 140±12 s for the short acquisition (P<0.0001). DLR images had higher sharpness compared to non-DLR (P<0.001). Short and short-DLR had lower SNR than the standard and standard-DLR (P<0.001). The perceived image quality of short-DLR was rated better in all categories compared to the standard sequence (P<0.001 to P=0.004). All domains of subjective evaluation were correlated with measured image sharpness (P<0.001).

Conclusions: T2-TSE acquisition of the prostate accelerated using CS combined with DLR reconstruction provides images with increased sharpness that have a superior quality as perceived by human readers compared to standard T2-TSE. The perceived image quality is correlated with measured image contrast.

Keywords: Magnetic resonance imaging (MRI); prostate cancer; artificial intelligence (AI); image reconstruction

Submitted Oct 23, 2023. Accepted for publication Mar 14, 2024. Published online Apr 11, 2024.
doi: 10.21037/qims-23-1488
View this article at: https://dx.doi.org/10.21037/qims-23-1488

^ ORCID: Lukas Lambert, 0000-0003-2299-4707; Andrea Burgetova, 0000-0002-9975-2338.

Introduction

Magnetic resonance imaging (MRI) of the prostate has been introduced in the pathway of early detection of clinically significant prostate cancer (csPCa) alongside serum prostate-specific antigen (PSA) levels and digital rectal examination to improve the efficiency of the process (1,2). Even risk-stratified population screening for prostate MRI places a substantial strain on the MR facilities where it competes for scanner time (3).

To maintain the image quality of multiparametric MRI (mpMRI), the acquisition protocol should reflect recommendations set by the Prostate Imaging Reporting and Data System (PI-RADS) 2.1 working group (4) and fulfill criteria set by the PI-QUAL (5). To simplify and accelerate prostate imaging, it has been suggested that bi-parametric MRI (bpMRI) may not be inferior in the detection of csPCa compared to mpMRI in a selected population (3,6). The use of a 3D T2-weighted turbo-spin-echo (TSE) sequence to replace the three planes commonly used for T2 imaging of the prostate has been proposed but has not been widely adopted due to lower spatial resolution, greater susceptibility to motion artifacts, and worse tissue contrast compared to T2-TSE (7). Also, reducing the imaging to only one plane spares additional time with diagnostic accuracy comparable to "full" bi-plane T2 imaging in a so-called "fast bpMRI" (8,9).

Great effort has also been devoted to the acceleration of MRI sequences including improved signal processing, parallel imaging techniques, improved coil geometry, and sensitivity. Variable density pseudo-random k-space undersampling along the phase encoding direction with wavelet sparsity constraint and image reconstruction using sensitivity encoding parallel imaging ("compressed sensing", CS) allow further temporal optimization of an MRI sequence, sometimes with aggravation of image artifacts (10-12). Image reconstruction from subsampled data using artificial intelligence (AI) and specifically deep-learning-based reconstruction (DLR) has introduced another dimension of optimization of acquisition time, and the body of literature describing its potential in accelerating prostate MRI is growing (13-17).

Methods for reconstructing MR images from undersampled data based on deep learning include a variety of approaches, including popular architectures such as U-Net, implemented either as dual-domain networks to exploit both spatial and k-space information or separately. Additionally, the utilization of Recurrent Neural Networks (RNN) or Generative Adversarial Networks (GAN) is common in MR image reconstruction. Hybrid methodologies integrate deep learning with physical models, iteratively refining the reconstruction process (18).

Only one study has previously used DLR with resolution upscaling convolutional neural network (CNN) to improve images acquired with low resolution (19). Here, we used both of these techniques for standard acquisition and its accelerated version changing the CS acceleration factor.

The recently developed SuperResolution CNN for upscaling magnetic resonance (MR) images is being implemented in clinical imaging and requires validation along with other acquisition and reconstruction techniques. Several studies have evaluated the performance of different types of SuperResolution networks using deep neural networks for brain MRI in terms of diagnostic performance and image quality (20-22). Novel denoising and super-resolution approaches for MR images have been proposed and integrated into a single framework (23). GAN-based SR methods have also been reviewed for MRI reconstruction and acceleration tasks (24). Deep learning has been explored for enhancing spatial detail from small-matrix MRI acquisitions and has shown promising results.

The objective of this study was to compare the image quality of standard and accelerated T2 TSE of the prostate reconstructed with and without DLR (including resolution upscaling CNN) and to find associations between perceived image quality and calculated image characteristics. We present this article in accordance with the STROBE reporting checklist (available at https://qims.amegroups.com/article/view/10.21037/qims-23-1488/rc).

Methods

The study was conducted in accordance with the Declaration of Helsinki (as revised in 2013). The study was approved by Ethics Committee of the General University Hospital in Prague (No. 244/21 S-IV) and informed consent was taken from all individual participants.

Patient population

In this observational prospective study, we included consecutive patients ≥45 years of age who underwent bpMRI of the prostate for suspected prostate cancer between October 25, 2022, and December 2, 2022. The inclusion criteria were: informed consent; age ≥45 years; bpMRI; raw data and subsequent complete reconstructions

Table 1 Acquisition and reconstruction protocols

Acquisition	Std/Short
Acquisition time (min:s)	4:27/2:13
Field-of-view (mm)	230×184
Acquisition voxel size (mm)	0.62×0.76
Slice thickness (mm)	3
Slice gap	0
Number of slices	38
Number of excitations	1
Acquisition matrix	372×299
TE (ms)	100
TR (s)	3.9
TSE factor	15
Bandwidth (Hz)	143
Compressed sense factor	1.3/2.8
Plane	Transverse
Phase encoding	RL
Reconstruction matrix	Std: 400; DLR: 1,008

Std, standard acquisition; Short, short acquisition; TE, time to echo; TR, repetition time; TSE, turbo spine echo; DLR, deep-learning-based reconstruction; RL, right-left.

of both short and long T2-TSE acquisitions. Exclusion criteria were: prior prostatectomy; and severe artifacts from motion or metallic implants on T2-TSE.

MR acquisition

The examinations were performed on a 3T MRI scanner, Ingenia Elition (Philips, Best, The Netherlands), using phased array coils. Before the examination, all patients received hyoscine butylbromide (Buscopan, Boehringer Ingelheim Espana SA, Sant Cugat Del Valles, Spain) 20 mg/1 mL i.v. Within the bi-parametric prostate MRI, two transverse T2-TSE sequences were acquired (*Table 1*). The acquisition time of a standard T2-TSE sequence had an estimated time of 4:27 s. The short T2 sequence (short) was accelerated twice using CS with an estimated acquisition time of 2:13 s. During the study interval, the order in which the two acquisitions were made, was changed.

The data were immediately reconstructed with currently available CS technique (11,12,25-27). CS performs variable density pseudo-random k-space undersampling along the phase encoding direction. CS reconstruction algorithm performs iterative wavelet transformation of major components with wavelet sparsity constraint, suppression of noise, and comparison with original acquisition. CS is used together with parallel imaging technique (sensitivity encoding).

Raw data from the two acquisitions were saved and additionally reconstructed using vendor provided prototype (Philips SmartSpeed Precise Image, *Table 1*). This AI-based reconstruction technique consists of a series of CNNs as Adaptive CS Network (28) and SuperResolution Network (Precise Image Network) (29).

Adaptive CS Network represents iterative shrinkage-thresholding approach (ISTA) as presented by Zhang *et al.* (30) and allows to reconstruct images acquired with CS technique (18,31,32).

This CNN is applied prior coil channel combination, removing the noise from the images to obtain good image quality from accelerated acquisitions (29). The Adaptive-CS-Network employed in this work was pre-trained on 740,000 sparsifying MR images using both 1.5T and 3T images of various anatomies and contrasts (25,33). The prototype was adapted and optimized to run on up-to-date standard reconstruction hardware available in our 3T MR scanner (31).

Precise Image Net is an AI-model applied to remove ringing artefacts and to replace the traditional zero-filling strategy to increase the matrix size and therewith the sharpness of the images; these types of networks are known as Super Resolution networks (34,35). This network is trained on pairs of low- and high-resolution data with k-space crops to induce ringing. Data consistency checks are implemented to match the resulting k-space with the measured k-space data. The full reconstruction pipeline generates images with improved signal-to-noise ratio (SNR) and sharpness, higher matrix size and reduced ringing artefacts, and can be applied to all two-dimensional (2D) cartesian acquisitions.

MR evaluation and data processing

The studies were transferred to a multimodality workstation (Intellispace Portal, Philips, Best, The Netherlands) and reviewed in a random order. Three radiologists with experience of 4, 10, and 12 years in prostate MRI imaging (I.M., M.W., A.B.) rated the image quality on a five-point scale as (I) non-diagnostic; (II) poor but still interpretable; (III) acceptable (worse than expected); (IV) good (as

Table 2 Patient's characteristics

Parameter	Value
Patients (n)	47
Age (years) (mean ± SD)	69.8±8.3
MRI request (n)	
Suspected prostate cancer (PSA ± DRE)	37
Known prostate cancer	
After TURP	2
Before radiotherapy	4
Active surveillance	4
Prostate volume (mL) (mean ± SD)	69.8±8.3
PI-RADS (n)	
Not stated	5
1	0
2	30
3	4 (4 PZ)
4	7 (7 PZ)
5	1 (1 PZ)

SD, standard deviation; MRI, magnetic resonance imaging; PSA, prostate specific antigen; DRE, digital rectal examination; TURP, transurethral resection of the prostate; PI-RADS, Prostate Imaging-Reporting and Data System; PZ, peripheral zone.

expected); (V) excellent (better than expected) in the following categories: (i) image noise; (ii) image contrast; (iii) image sharpness; (iv) neurovascular bundle delineation; (v) urethral sphincter delineation; (vi) overall image quality (7,36). They also rated the presence of motion artifacts on a five-point scale to exclude acquisitions deteriorated by motion (non-interpretable, or poor but still interpretable).

One radiologist (M.W.) measured (I) mean and standard deviation of voxel intensity in an oval region of interest (ROI) in the fat tissue in the ischiorectal fossa on the right and left side, and (II) volume of the prostate (37,38).

For objective quantification of image sharpness, the mean absolute value of the intensity gradient was computed for each slice after it was cropped to the central 50% in both dimensions. This computation utilized a 2D discrete differential operator, considering the pixel size to enable accurate comparisons. These determined values of the image gradient magnitude reflect the steepness of the signal intensity edges, which is strongly correlated with image sharpness, as previously demonstrated (39). This value reflects the steepness of signal intensity edges, which strongly correlates with image sharpness. The computation was implemented in Python 3.9, operating in fully automatic mode. The source code for this implementation was made available in the GitHub repository (https://github.com/JakubicekRoman/QuantSharp). SNR was calculated as average signal intensity in the right and left ischiorectal fossa divided by its standard deviation.

Clinical data were retrieved from the hospital information system, and radiology reports, that were searched for previous prostate surgery, for the reason to perform MRI, and PI-RADS score (4).

Based on the sample size calculation to achieve a power of 80% and a two-sided level of significance of 5% for an effect size of 0.5, the study required 34 subjects.

Statistical analysis

Statistical analysis was performed in Prism (GraphPad Software, La Jolla, CA, USA), and R (R Foundation for Statistical Computing, Vienna, Austria). Continuous and ordinal data were compared using the Friedman's test with Nemenyi's post hoc tests, and expressed as median (interquartile range, IQR) or average ± standard deviation according to their distribution (D'Agostino & Pearson omnibus normality test). Average values of subjective evaluation scores were compared. Correlations were calculated using Spearman rank correlation ("rho", ρ). Interobserver agreement was calculated as Fleiss' kappa. A P value <0.05 was considered significant.

Results

From 48 bpMRI complete consecutive MR acquisitions (standard and short) and reconstructions (standard and DLR), one study was excluded due to severe motion artifacts, yielding a final study group of 47 patients 69.8±8.3 years old. MRI was requested for suspected prostate cancer (n=37), known prostate cancer after transurethral prostate resection (n=2), before radiotherapy (n=4), or as active surveillance (n=4, *Table 2*). The mean acquisition time was 281±23 s for the standard and 140±12 s for the short sequence.

The perceived image quality (*Figure 1*) was rated better in all categories in the short-DLR sequence compared to the standard sequence (without DLR, P<0.001 to P=0.004). No significant difference was observed between standard-DLR and short-DLR or standard and short sequences (*Figure 2*, Table S1). Images reconstructed with

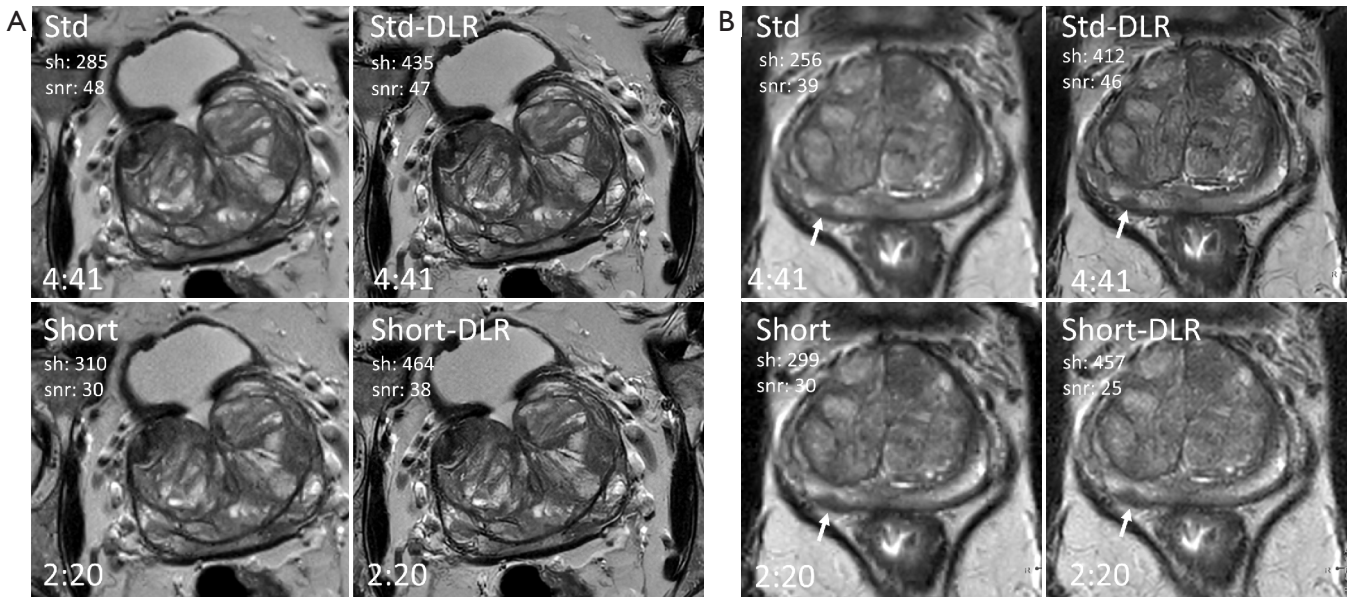

Figure 1 Comparison among standard and short T2 weighted turbo spin echo acquisitions and reconstructions with and without deep learning in 82-year-old (A) and 73-year-old (B) patients with well delineated hyperplastic nodules in the transition zone. PI-RADS 4 lesion in the peripheral zone of the right posterior midgland (Gleason score 4+4, arrow) and mild motion blur can be appreciated in the second patient (B). Std, standard acquisition; sh, sharpness; snr, signal-to-noise ratio; Short, short acquisition; DLR, deep-learning-based reconstruction; PI-RADS, Prostate Imaging-Reporting and Data System.

DLR had significantly better sharpness compared to non-DLR reconstructions (P<0.001, Table S1, *Figure 3*). Even short acquisition with DLR had a better image sharpness than standard acquisition without DLR (P<0.001). No difference in SNR was observed between DLR and standard reconstruction both in the short acquisitions (P=0.53) or in the standard acquisitions (P=0.91). Both short and short-DLR had lower SNR compared to the standard and standard-DLR (P<0.001).

All categories of subjective evaluation were highly correlated with measured image sharpness (P<0.001, Table S2). SNR was correlated with image noise (P<0.001), image contrast (P=0.04), image sharpness (P=0.03), and overall rating of image quality (P<0.001, Table S2).

The Interobserver agreement in rating image quality in the six domains ranged from 0.49 (image contrast) to 0.72 (image sharpness, Table S3).

Discussion

In this prospective study, we showed that DLR reconstruction with resolution upscaling in both standard and short T2 TSE acquisitions improved image sharpness and perceived image quality in all domains. The DLR image even from the short acquisition was rated superior to the standard acquisition without DLR.

DLR is based on deep learning performed on an artificial neural network. The network develops associations between undersampled data from K-space and their standard equivalents (supervised learning). Also, AI performs unsupervised learning that enforces data consistency and suppresses artifacts (40,41). Finally, the network reaches a state, where it reproduces heavily undersampled data in MRI images with nearly original image quality.

In this work, we studied the influence of image acquisition (acceleration by sparse K-space sampling) and reconstruction (with and without DLR) on image quality. We demonstrated the positive effect of DLR especially on the image sharpness and perceived image quality. Previously, Gassenmaier *et al.* reported the use of DLR in three-plane prostate T2-TSE with the acceleration of the whole protocol by a factor of 2.7 and improved perceived image quality (13). The same study group reported improved perceived image quality using 2 mm instead of 3 mm slice thickness reconstructed using DLR (42). Their evaluation of image quality was based on a devised

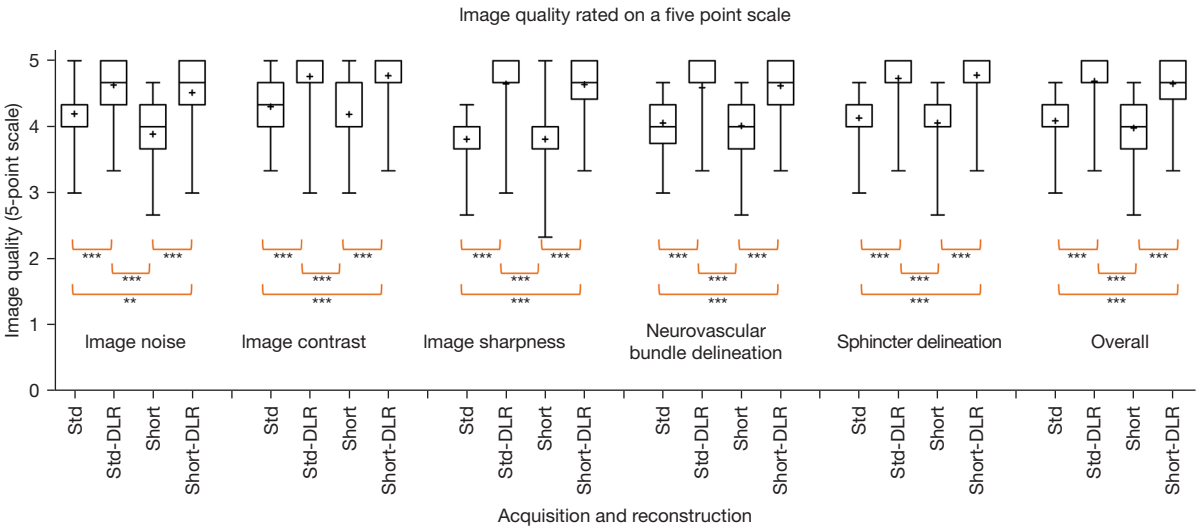

Figure 2 Comparison of image quality rated on a five-point scale on a box-and-whiskers plot (min, lower quartile, median, upper quartile, max, '+' denotes average) among standard and short acquisition protocols and reconstruction with and without deep learning. Post-hoc tests significance is marked by asterisks: ***, P<0.001; **, P<0.01. Std, standard acquisition; Short, short acquisition; DLR, deep-learning-based reconstruction.

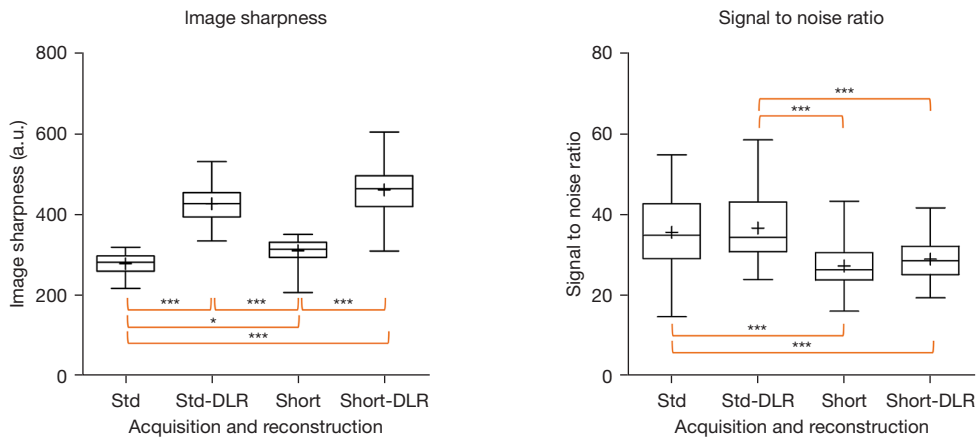

Figure 3 Comparison of measured image sharpness and contrast-to-noise ratio on a box-and-whiskers plot (min, lower quartile, median, upper quartile, max, '+' denotes average) among standard and short acquisition protocols and reconstruction with and without deep learning. Post-hoc tests significance is marked by asterisks: ***, P<0.001; *, P<0.05. a.u., arbitrary unit; Std, standard acquisition; DLR, deep-learning-based reconstruction; Short, short acquisition.

four-point scale and no objective evaluation was performed. The use of DLR affected neither the T2 score nor the overall PI-RADS category. In our study, a time reduction by a factor of 2 was tested with similar results on a different 3T scanner. We also showed that DLR substantially improved image sharpness both in standard and accelerated sequences. Harder *et al.* compared undersampled T2-TSE with different acceleration factors using compressed sense and earlier version of DLR on a six-point Likert scale in six dimensions and with apparent SNR, CNR, and line profile. They showed that DLR lead to increased SNR, CNR and image quality ratings enabling 58% acceleration (25).

Lee *et al.* reported that T2-TSE accelerated by 33% by reducing the number of excitations from 1.5 to 1 and reconstructed with DLR did not compromise image quality compared to the standard of care (16). Kim *et al.*

found that T2-TSE accelerated by a factor of four even if reconstructed with DLR results in lower ratings of image quality compared to the standard of care (15). Park *et al.* showed that fast T2-TSE reconstructed with DLR had higher SNR, but in our study, DLR improved sharpness but not SNR (43). Another study by Tong *et al.* reported two to three-fold acceleration of T2-TSE using DLR with preserved image quality (44). Johnson *et al.* used retrospective synthetic undersampling of T2-TSE with computed acceleration of scan time by a factor of six (14). A significant difference in overall image quality was regarded by only one of their four readers, but the diagnostic performance in the identification of clinically significant lesions did not change. In our study, we did not evaluate the diagnostic performance, because none of the patients had any clinically significant lesion in the transition zone, where T2 sequence is dominant for its evaluation. Although previous studies claimed to have addressed the diagnostic performance as well, the number of evaluated significant lesions in the transition zone was limited (19,25).

Recently, Bischoff *et al.* published a study comparing T2-TSE with decreased resolution reconstructed with DLR including resolution upscaling using similar reconstruction software acquired with 36% time save and improved image sharpness (19). In this study, we used the SuperResolution net to upscale images acquired with standard resolution.

Although the image quality can be objectively (homogeneity, resolution, linearity, SNR) measured on an MRI phantom, it rarely resembles the heterogeneous landscape introduced by the human body including motion and susceptibility artifacts. Excellent image quality of T2-TSE of the prostate can be obtained even without respecting minimal parameters recommended by the PI-RADS v2.1 (4,5). Apart from the technical capabilities of the scanner, the image quality of prostate T2-TSE is also affected by other settings (e.g. bandwidth, turbo factor, echo and repetition times, voxel size, slice thickness) and other factors including motion artifacts, susceptibility artifacts, and patient diameter (5,45).

Rating of image quality was systematically introduced by Giganti *et al.* as PI-QUAL score (5,36). The score is also based on subjective evaluation only. Objective image quality measurement on MRI in different domains is difficult, although the use of AI in quality control of prostate MRI has been proposed (46). Here, we expressed sharpness in absolute values as a no-reference statistics of gradient of the edges (39). In accordance with the PI-QUAL scoring system, image quality is perceived as image sharpness rather more than SNR.

Study limitations

We identified the following limitations of the study. First, we evaluated only one sequence of the bi-parametric MRI protocol. Second, although the sequence of standard and short acquisitions was alternated, the difference in the appearance of the images was revealing of the reconstruction algorithm. Third, this study was performed on a technical level as none of these patients had clinically significant lesions in the transition zone, where the T2 sequence is dominant for interpretation. Fourth, the reconstruction of DLR in research mode had to be performed from raw data in off-time (research software) and therefore 9 patients with incomplete DLR reconstructions (auto-deleted raw data or DLR reconstruction not completed) could not be included. Further studies should ensue to evaluate the effect of short MRI acquisition with DLR on the diagnostic performance of prostate MRI in the transition zone, where the T2 sequence is dominant.

Conclusions

Acceleration of T2 TSE prostate MRI by a factor of two using CS combined with deep learning reconstruction produces images with increased sharpness that have a superior quality as perceived by human readers compared to standard T2-TSE. The perceived image quality is correlated with measured image sharpness.

Acknowledgments

Funding: This study was supported by the Ministry of Health of the Czech Republic (MH CZ-DRO, General University Hospital in Prague) (No. 00064165) and the institutional funding of the Charles University in Prague (Cooperatio, Medical Diagnostics and Basic Medical Sciences) (UNCE 24/MED/018).

Footnote

Reporting Checklist: The authors have completed the STROBE reporting checklist. Available at https://qims.amegroups.com/article/view/10.21037/qims-23-1488/rc

Conflicts of Interest: All authors have completed the ICMJE uniform disclosure form (available at https://qims.

amegroups.com/article/view/10.21037/qims-23-1488/coif). L.L. serves as an unpaid editorial board member of *Quantitative Imaging in Medicine and Surgery*. P.O. is a current employee of Philips Healthcare. The other authors have no conflicts of interest to declare.

Ethical Statement: The authors are accountable for all aspects of the work in ensuring that questions related to the accuracy or integrity of any part of the work are appropriately investigated and resolved. The study was conducted in accordance with the Declaration of Helsinki (as revised in 2013). The study was approved by Ethics Committee of the General University Hospital in Prague (No. 244/21 S-IV) and informed consent was taken from all individual participants.

References

1. Eldred-Evans D, Tam H, Sokhi H, Padhani AR, Winkler M, Ahmed HU. Rethinking prostate cancer screening: could MRI be an alternative screening test? Nat Rev Urol 2020;17:526-39.
2. Frisbie JW, Van Besien AJ, Lee A, Xu L, Wang S, Choksi A, Afzal MA, Naslund MJ, Lane B, Wong J, Wnorowski A, Siddiqui MM. PSA density is complementary to prostate MP-MRI PI-RADS scoring system for risk stratification of clinically significant prostate cancer. Prostate Cancer Prostatic Dis 2023;26:347-52.
3. Wallström J, Geterud K, Kohestani K, Maier SE, Månsson M, Pihl CG, Socratous A, Arnsrud Godtman R, Hellström M, Hugosson J. Bi- or multiparametric MRI in a sequential screening program for prostate cancer with PSA followed by MRI? Results from the Göteborg prostate cancer screening 2 trial. Eur Radiol 2021;31:8692-702.
4. Turkbey B, Rosenkrantz AB, Haider MA, Padhani AR, Villeirs G, Macura KJ, Tempany CM, Choyke PL, Cornud F, Margolis DJ, Thoeny HC, Verma S, Barentsz J, Weinreb JC. Prostate Imaging Reporting and Data System Version 2.1: 2019 Update of Prostate Imaging Reporting and Data System Version 2. Eur Urol 2019;76:340-51.
5. Giganti F, Kasivisvanathan V, Kirkham A, Punwani S, Emberton M, Moore CM, Allen C. Prostate MRI quality: a critical review of the last 5 years and the role of the PI-QUAL score. Br J Radiol 2022;95:20210415.
6. Bass EJ, Pantovic A, Connor M, Gabe R, Padhani AR, Rockall A, Sokhi H, Tam H, Winkler M, Ahmed HU. A systematic review and meta-analysis of the diagnostic accuracy of biparametric prostate MRI for prostate cancer in men at risk. Prostate Cancer Prostatic Dis 2021;24:596-611.
7. Polanec SH, Lazar M, Wengert GJ, Bickel H, Spick C, Susani M, Shariat S, Clauser P, Baltzer PAT. 3D T2-weighted imaging to shorten multiparametric prostate MRI protocols. Eur Radiol 2018;28:1634-41.
8. van der Leest M, Israël B, Cornel EB, Zámecnik P, Schoots IG, van der Lelij H, Padhani AR, Rovers M, van Oort I, Sedelaar M, Hulsbergen-van de Kaa C, Hannink G, Veltman J, Barentsz J. High Diagnostic Performance of Short Magnetic Resonance Imaging Protocols for Prostate Cancer Detection in Biopsy-naïve Men: The Next Step in Magnetic Resonance Imaging Accessibility. Eur Urol 2019;76:574-81.
9. Hötker AM, Vargas HA, Donati OF. Abbreviated MR Protocols in Prostate MRI. Life (Basel) 2022;12:552.
10. Winkel DJ, Heye TJ, Benz MR, Glessgen CG, Wetterauer C, Bubendorf L, Block TK, Boll DT. Compressed Sensing Radial Sampling MRI of Prostate Perfusion: Utility for Detection of Prostate Cancer. Radiology 2019;290:702-8.
11. Yu VY, Zakian K, Tyagi N, Zhang M, Romesser PB, Dresner A, Cerviño L, Otazo R. Combined Compressed Sensing and SENSE to Enhance Radiation Therapy Magnetic Resonance Imaging Simulation. Adv Radiat Oncol 2022;7:100799.
12. Lustig M, Donoho D, Pauly JM. Sparse MRI: The application of compressed sensing for rapid MR imaging. Magn Reson Med 2007;58:1182-95.
13. Gassenmaier S, Afat S, Nickel MD, Mostapha M, Herrmann J, Almansour H, Nikolaou K, Othman AE. Accelerated T2-Weighted TSE Imaging of the Prostate Using Deep Learning Image Reconstruction: A Prospective Comparison with Standard T2-Weighted TSE Imaging. Cancers (Basel) 2021;13:3593.
14. Johnson PM, Tong A, Donthireddy A, Melamud K, Petrocelli R, Smereka P, Qian K, Keerthivasan MB, Chandarana H, Knoll F. Deep Learning Reconstruction Enables Highly Accelerated Biparametric MR Imaging of

the Prostate. J Magn Reson Imaging 2022;56:184-95.
15. Kim EH, Choi MH, Lee YJ, Han D, Mostapha M, Nickel D. Deep learning-accelerated T2-weighted imaging of the prostate: Impact of further acceleration with lower spatial resolution on image quality. Eur J Radiol 2021;145:110012.
16. Lee KL, Kessler DA, Dezonie S, Chishaya W, Shepherd C, Carmo B, Graves MJ, Barrett T. Assessment of deep learning-based reconstruction on T2-weighted and diffusion-weighted prostate MRI image quality. Eur J Radiol 2023;166:111017.
17. Ghodrati V, Shao J, Bydder M, Zhou Z, Yin W, Nguyen KL, Yang Y, Hu P. MR image reconstruction using deep learning: evaluation of network structure and loss functions. Quant Imaging Med Surg 2019;9:1516-27.
18. Wang S, Xiao T, Liu Q, Zheng H. Deep learning for fast MR imaging: A review for learning reconstruction from incomplete k-space data. Biomed Signal Process Control 2021;68:102579.
19. Bischoff LM, Peeters JM, Weinhold L, Krausewitz P, Ellinger J, Katemann C, Isaak A, Weber OM, Kuetting D, Attenberger U, Pieper CC, Sprinkart AM, Luetkens JA. Deep Learning Super-Resolution Reconstruction for Fast and Motion-Robust T2-weighted Prostate MRI. Radiology 2023;308:e230427.
20. Sharma R, Tsiamyrtzis P, Webb AG, Seimenis I, Loukas C, Leiss E, Tsekos NV. A Deep Learning Approach to Upscaling "Low-Quality" MR Images: An In Silico Comparison Study Based on the UNet Framework. Appl Sci 2022;12:11758.
21. Zhou Z, Ma A, Feng Q, Wang R, Cheng L, Chen X, Yang X, Liao K, Miao Y, Qiu Y. Super-resolution of brain tumor MRI images based on deep learning. J Appl Clin Med Phys 2022;23:e13758.
22. Terada Y, Miyasaka T, Nakao A, Funayama S, Ichikawa S, Takamura T, Tamada D, Morisaka H, Onishi H. Clinical evaluation of super-resolution for brain MRI images based on generative adversarial networks. Inform Med Unlocked 2022;32:101030.
23. Kaur P, Sao AK, Ahuja CK. Super Resolution of Magnetic Resonance Images. J Imaging 2021;7:101.
24. Guerreiro J, Tomás P, Garcia N, Aidos H. Super-resolution of magnetic resonance images using Generative Adversarial Networks. Comput Med Imaging Graph 2023;108:102280.
25. Harder FN, Weiss K, Amiel T, Peeters JM, Tauber R, Ziegelmayer S, Burian E, Makowski MR, Sauter AP, Gschwend JE, Karampinos DC, Braren RF. Prospectively Accelerated T2-Weighted Imaging of the Prostate by Combining Compressed SENSE and Deep Learning in Patients with Histologically Proven Prostate Cancer. Cancers (Basel) 2022.
26. Geerts-Ossevoort L, de Weerdt E, Duijndam A, van IJperen G, Peeters H, Doneva M, Nijenhuis M, Huang A. Speed done right. Every time. 2020. Accessed 9 Oct 2023. Available online: https://www.philips.com.vn/c-dam/b2bhc/master/landing-pages/compressed-sense-redesign/speed/MR_white_paper_Compressed_SENSE.pdf
27. Hollingsworth KG. Reducing acquisition time in clinical MRI by data undersampling and compressed sensing reconstruction. Phys Med Biol 2015;60:R297-322.
28. Pezzotti N, Yousefi S, Elmahdy MS, Van Gemert JHF, Schuelke C, Doneva M, Nielsen T, Kastryulin S, Lelieveldt BPF, Van Osch MJP, De Weerdt E, Staring M. An Adaptive Intelligence Algorithm for Undersampled Knee MRI Reconstruction. IEEE Access 2020;8:204825-38.
29. Peeters H, Chung H, Valvano G, Yakisikli D, van Gemert J, de Weerdt E, van de Ven K. Philips SmartSpeed. No compromise Image quality and speed at your fingertips. Accessed 9 Oct 2023. Available online: https://images.philips.com/is/content/PhilipsConsumer/Campaigns/HC20140401_DG/Documents/HC05072022-white_paper_philips_smartspeed.pdf
30. Zhang J, Ghanem B. ISTA-Net: Interpretable optimization-inspired deep network for image compressive sensing. 2018 IEEE/CVF Conference on Computer Vision and Pattern Recognition, Salt Lake City, UT, USA, 2018:1828-37.
31. Fervers P, Zaeske C, Rauen P, Iuga AI, Kottlors J, Persigehl T, Sonnabend K, Weiss K, Bratke G. Conventional and Deep-Learning-Based Image Reconstructions of Undersampled K-Space Data of the Lumbar Spine Using Compressed Sensing in MRI: A Comparative Study on 20 Subjects. Diagnostics (Basel) 2023;13:418.
32. Feuerriegel GC, Weiss K, Kronthaler S, Leonhardt Y, Neumann J, Wurm M, Lenhart NS, Makowski MR, Schwaiger BJ, Woertler K, Karampinos DC, Gersing AS. Evaluation of a deep learning-based reconstruction method for denoising and image enhancement of shoulder MRI in patients with shoulder pain. Eur Radiol 2023;33:4875-84.
33. Foreman SC, Neumann J, Han J, Harrasser N, Weiss K, Peeters JM, Karampinos DC, Makowski MR, Gersing AS, Woertler K. Deep learning-based acceleration of Compressed Sense MR imaging of the ankle. Eur Radiol 2022;32:8376-85.
34. Dong C, Loy CC, He K, Tang X. Image Super-Resolution

Using Deep Convolutional Networks. IEEE Trans Pattern Anal Mach Intell 2016;38:295-307.
35. Li Y, Sixou B, Peyrin F. A review of the deep learning methods for medical images super resolution problems. IRBM 2021;42:120-33.
36. Giganti F, Allen C, Emberton M, Moore CM, Kasivisvanathan V; PRECISION study group. Prostate Imaging Quality (PI-QUAL): A New Quality Control Scoring System for Multiparametric Magnetic Resonance Imaging of the Prostate from the PRECISION trial. Eur Urol Oncol 2020;3:615-9.
37. Zhang Z, Dai G, Liang X, Yu S, Li L, Xie Y. Can Signal-to-Noise Ratio Perform as a Baseline Indicator for Medical Image Quality Assessment. IEEE Access 2018;6:11534-43.
38. Erdogmus D, Larsson EG, Yan R, Principe JC, Fitzsimmons JR. Measuring the signal-to-noise ratio in magnetic resonance imaging: a caveat. Signal Process 2004;84:1035-40.
39. Zhan Y, Zhang R. No-Reference Image Sharpness Assessment Based on Maximum Gradient and Variability of Gradients. IEEE Trans Multimed 2018;20:1796-808.
40. Lin DJ, Johnson PM, Knoll F, Lui YW. Artificial Intelligence for MR Image Reconstruction: An Overview for Clinicians. J Magn Reson Imaging 2021;53:1015-28.
41. Chen Y, Schönlieb C-B, Liò P, Leiner T, Dragotti PL, Wang G, Rueckert D, Firmin D, Yang G. AI-based Reconstruction for Fast MRI -- A Systematic Review and Meta-analysis. Proceedings of the IEEE 2022;110:224-45.
42. Gassenmaier S, Warm V, Nickel D, Weiland E, Herrmann J, Almansour H, Wessling D, Afat S. Thin-Slice Prostate MRI Enabled by Deep Learning Image Reconstruction. Cancers (Basel) 2023;15:578.
43. Park JC, Park KJ, Park MY, Kim MH, Kim JK. Fast T2-Weighted Imaging With Deep Learning-Based Reconstruction: Evaluation of Image Quality and Diagnostic Performance in Patients Undergoing Radical Prostatectomy. J Magn Reson Imaging 2022;55:1735-44.
44. Tong A, Bagga B, Petrocelli R, Smereka P, Vij A, Qian K, Grimm R, Kamen A, Keerthivasan MB, Nickel MD, von Busch H, Chandarana H. Comparison of a Deep Learning-Accelerated vs. Conventional T2-Weighted Sequence in Biparametric MRI of the Prostate. J Magn Reson Imaging 2023;58:1055-64.
45. Czyzewska D, Sushentsev N, Latoch E, Slough RA, Barrett T. T2-PROPELLER Compared to T2-FRFSE for Image Quality and Lesion Detection at Prostate MRI. Can Assoc Radiol J 2022;73:355-61.
46. Kim H, Kang SW, Kim JH, Nagar H, Sabuncu M, Margolis DJA, Kim CK. The role of AI in prostate MRI quality and interpretation: Opportunities and challenges. Eur J Radiol 2023;165:110887.

Cite this article as: Jurka M, Macova I, Wagnerova M, Capoun O, Jakubicek R, Ourednicek P, Lambert L, Burgetova A. Deep-learning-based reconstruction of T2-weighted magnetic resonance imaging of the prostate accelerated by compressed sensing provides improved image quality at half the acquisition time. Quant Imaging Med Surg 2024;14(5):3534-3543. doi: 10.21037/qims-23-1488

Supplementary

Table S1 Comparison of image quality rated on a five-point scale (5= better than expected, 1= non-interpretable), calculated image sharpness, and signal-to-noise ratio among Std and short acquisitions and reconstruction with and without deep learning

Acquisition-reconstruction	Median (95% CI)				P	Post-hoc					
	Std (A)	Std-DLR (B)	Short (C)	Short-DLR (D)		(A)-(B)	(A)-(C)	(A)-(D)	(B)-(C)	(B)-(D)	(C)-(D)
Subjective evaluation											
Image noise	4.3 (3.2 to 4.7)	4.7 (3.4 to 5.0)	4.0 (3.0 to 4.3)	4.7 (3.3 to 5.0)	<0.0001	<0.0001	0.052	0.0044	<0.0001	0.71	<0.0001
Image contrast	4.3 (3.5 to 4.7)	5.0 (3.6 to 5.0)	4.0 (3.4 to 4.7)	5.0 (3.6 to 5.0)	<0.0001	<0.0001	0.87	<0.0001	<0.0001	1.0	<0.0001
Image sharpness	4.0 (3.1 to 4.2)	4.7 (3.5 to 5.0)	4.0 (3.1 to 4.3)	4.7 (3.5 to 5.0)	<0.0001	<0.0001	1.0	<0.0001	<0.0001	1.0	<0.0001
NB delineation	4.0 (3.3 to 4.7)	4.7 (3.4 to 5.0)	4.0 (3.1 to 4.7)	4.7 (3.4 to 5.0)	<0.0001	<0.0001	0.98	<0.0001	<0.0001	1.00	<0.0001
Sphincter delineation	4.3 (3.3 to 4.7)	5.0 (3.5 to 5.0)	4.3 (3.1 to 4.7)	5.0 (3.5 to 5.0)	<0.0001	<0.0001	0.96	<0.0001	<0.0001	0.95	<0.0001
Overall	4.3 (3.1 to 4.7)	5.0 (3.4 to 5.0)	4.0 (3.1 to 4.7)	4.7 (3.4 to 5.0)	<0.0001	<0.0001	0.85	<0.0001	<0.0001	0.98	<0.0001
Objective measurements											
Image sharpness	282 (245 to 316)	428 (360 to 497)	314 (260 to 349)	465 (388 to 554)	<0.0001	<0.0001	0.029	<0.0001	<0.0001	0.38	<0.0001
Signal -to-noise ratio	37.2 (35.9 to 40.5)	38.0 (37.2 to 41.4)	28.0 (27.1 to 30.1)	30.2 (29.0 to 32.0)	<0.0001	0.91	<0.0001	<0.0001	<0.0001	<0.0001	0.53

Std, standard acquisition; Short, short acquisition; DLR, deep-learning-based reconstruction; 95% CI, 95% confidence interval; NB, neurovascular bundle.

Table S2 Cross-correlation matrix of objective measurements (image sharpness, signal-to-noise ratio, prostate volume) and subjective ratings

Parameter	Image sharpness		Signal-to-noise ratio		Volume	
	ρ	P	ρ	P	ρ	P
Subjective evaluation						
Image noise	0.438	<0.0001*	0.268	0.0002*	0.439	<0.0001*
Image contrast	0.612	<0.0001*	0.147	0.044*	0.612	<0.0001*
Image sharpness	0.657	<0.0001*	0.153	0.036*	0.657	<0.0001*
Neurovascular bundle delineation	0.517	<0.0001*	0.094	0.199	0.517	<0.0001*
Sphincter delineation	0.645	<0.0001*	0.136	0.062	0.645	<0.0001*
Overall	0.539	<0.0001*	0.195	0.0007*	0.539	<0.0001*
Objective measurements						
Image sharpness	–	–				
Signal-to-noise ratio	–0.016	0.83	–	–		
Prostate volume	0.002	0.97	–0.062	0.395	–	–

*, indicates statistical significance. ρ, Spearmann's rho.

Table S3 Interobserver agreement in domains of subjective rating of image quality

Domain	Agreement	95% CI
Image noise	0.53	0.44 to 0.60
Image contrast	0.49	0.39 to 0.59
Image sharpness	0.72	0.64 to 0.78
Overall	0.57	0.49 to 0.64
NB delineation	0.57	0.48 to 0.64
Sphincter delineation	0.54	0.44 to 0.63

95% CI, 95% confidence interval; NB, neurovascular bundle.